

Bone osteosarcoma tumor classification

Kamel Hussien Rahouma¹, Ahmed Salama Abdellatif²

¹Department of Electrical Engineering, Faculty of Engineering, University of Minia, Minia, Egypt

²Department of Mission Control Center, Egyptian Space Agency, Cairo, Egypt

Article Info

Article history:

Received Oct 20, 2022

Revised Mar 15, 2023

Accepted Mar 24, 2023

Keywords:

Deep learning

Ensemble voting

Gray level co-occurrence matrix

Image detection

Medical imaging

Osteosarcoma detection

ABSTRACT

Osteosarcoma is a malignant bone tumor that usually affects children and adolescents. Early detection of osteosarcoma tumors increases the likelihood of successful therapy. Manual identification of osteosarcoma requires highly skilled doctors. In this study, we attempt to create a model to automatically diagnose tumors into three categories; non-tumor, viable-tumor, and osteosarcoma tumor. The suggested methodology can help medical professionals identify tumors correctly and quickly. The proposed approach uses the gray level co-occurrence matrix (GLCM) to extract features for feature extraction and three different classifiers for tumor detection. The used classifier are XG-Boost, support vector machine (SVM), and K-nearest neighbors. Finally, ensemble voting is used by combining the predictions from these classifiers. The system achieves 91.8% accuracy.

This is an open access article under the [CC BY-SA](https://creativecommons.org/licenses/by-sa/4.0/) license.



Corresponding Author:

Ahmed Salama Abdellatif

Department of Mission Control Center, Egyptian Space Agency

Cairo, Egypt

Email: ah_salama_eng_eg@yahoo.com

1. INTRODUCTION

Cancer is a collection of disorders that can emerge as a result of abnormal cell proliferation, afterwards spreading to other regions of the body [1]. Osteosarcoma is the most common malignant tumor that can affect the long bone. Osteosarcoma accounts for 2% of all tumors in children aged up to 14, and 3% of tumors in adolescents aged 15 to 19. It is most commonly diagnosed between the ages of 10 and 30, with the majority of diagnoses happening in adolescence. However, osteosarcoma can strike at any age, including the elderly. About 10% of osteosarcoma cases are diagnosed in adults over the age of 60 [2]. Osteosarcoma tumors occur due to the growth of new bone tissue, This tissue is softer and weaker than regular bone tissue. Osteosarcoma is the most frequent kind of bone cancer. Osteosarcoma normally affects children from age of ten to fourteen years. Osteosarcoma tumors commonly appear in the leg; femur lower part or femur or tibia upper part [3]. Histologically, Osteosarcoma tumors are classified into two main categories benign or malignant tumors [4]. The dataset obtained by a team of clinical investigators from the University of Texas Southwestern Medical Center in Dallas will be used in this investigation [5], [6].

Osteosarcoma identification necessitates the use of highly experienced specialists as well as a significant amount of time. In order to diagnose osteosarcomas more accurately than computerized tomography (CT) scans and magnetic resonance imaging (MRI), researchers are already employing whole slide images (WSIs). Staining tissue samples from damaged regions with hematoxylin and eosin is one of the most used methods for identifying these cells. After staining, the samples are mounted on glass slides and examined by a pathologist under a microscope. In this research, we utilised high-quality WSIs, which are digital representations of glass slides with no pre-processing [7], [8].

Pathological assessment of tumor necrosis following treatment is critical for patients with osteosarcoma. When cancer is diagnosed in its early stages, treatment is more successful, and survival improves

dramatically. Nonetheless, 50% of cancers are still discovered at an advanced stage. Improved cancer diagnosis could significantly enhance survival rates. Despite the fact that recent improvements in early detection have saved lives [2]. In recent years artificial intelligence achieve great progress in image classification based on computer vision technology and has been widely employed successfully in various fields [9]. The computer vision usage helps specialists in early cancer diagnostic detection and also reduces human errors [10], [11].

Pathologists currently identify osteosarcoma using the staining technique. The doctors resect the affected parts, put them in a small glass then add a special type of stain to it. Normally, each stain type is used to diagnose specific diseases, for osteosarcoma hematoxylin and eosin (H&E) stains are used [12]. Finally, a specialist with high experience examines the slides under a microscope. In this work, we will use computer vision to detect osteosarcoma instead of using a microscope, so the conversion of glass slides to WSI digital image datasets is done. The WSI images differ from other digital images as their resolution is very high in addition the image characteristics depend on texture, color, and pattern [13].

Grey level co-occurrence matrices (GLCM) are one of the powerful techniques for image texture analysis that is applicable to WSI images [14], [15]. In this work, we will utilize GLCM for feature extraction and three different classifiers; XG-Boost, support vector machine (SVM), and K-nearest neighbors used for classification [16]-[17]. Finally, the ensemble-voting classifier is used [18], [19].

The remaining portions of the paper are organised as: section 2 briefly mentions some related work for osteosarcoma image classification. Section 3 will discuss the methods used in this work. Section 4 describes the proposed model methodology and results. Section 5 shows the obtained results. Finally, section 6 presents the work conclusion.

2. RELATES WORK

In this section, we will discuss some of the most relevant related work to our approach, e.g. osteosarcoma bone classification. Nabid *et al.* [20] suggested a model for osteosarcoma histological images using a sequential recurrent convolutional neural network (RCNN). The model consists of four histology region convolution (HRC) blocks and recurrent neural network-based bidirectional gated recurrent units (GRU) blocks. The model was evaluated by five-fold cross-validation by using five well-known different classifiers; AlexNet, ResNet50, VGG16, LeNet, and SVM machine learning techniques. The model provides an accuracy of 89%. Mahore *et al.* [21] Use four different machine learning algorithms to classify osteosarcoma into viable, necrotic, and non-tumor. The algorithms used are decision tree, SVM, K-nearest neighbors and adaptive boosting. The overall accuracy was 81.22%, 83.80%, 86.90%, and 91.70% for the decision tree, SVM, K-nearest neighbors, and adaptive boosting respectively. Ahmed *et al.* [22] present an automatic osteosarcoma histology image classification system based on CNN. The suggested approach consists of four modules: Modules for dataset collection, balancing imbalanced classes, classifying histology images, and evaluating CNN models. The training and testing accuracy of the non-regularized CNN model are 98% and 78% with an imbalanced dataset, and 96% and 81% with a balanced dataset, respectively. For an imbalanced dataset, the regularised CNN model's training and testing accuracies are 84% and 75%, respectively, whereas for a balanced dataset, they are 87% and 86%.

3. MATERIALS AND METHODS

3.1. Dataset description

The dataset was made up of histology photographs of osteosarcomas stained with hematoxylin and eosin (H&E). The information was acquired by a group of clinical experts from the University of Texas Southwestern Medical Center in Dallas. This dataset was created using archival samples from 50 kids treated at Children's Medical Center in Dallas between 1995 and 2015. Pathologists selected four patients (from a total of 50) based on the diversity of tumor specimens discovered following surgical resection. Each picture is labelled as non-tumor, viable tumor, or necrosis based on the most common kind of cancer that is present in that image. Two doctors worked together to annotate the text. Two pathologists each received a set of photos for the annotation activity. Since only one pathologist annotated any given image, each image only had one annotation. This dataset consists of 1091 images with a magnification of 10X and a size of 1024X1024. The distribution of the images is as: 292 viable tumor tiles, 263 necrotic tumors (osteosarcoma) images, and 536 non-tumor images. Figure 1 shows samples of images inside the used dataset. Figure 1(a) shows a sample image for norm bone. Figure 1(b) shows a sample image for bone that affected by viable tumor. Figure 1(c) shows a sample image for bone that affected by osteosarcoma tumor.

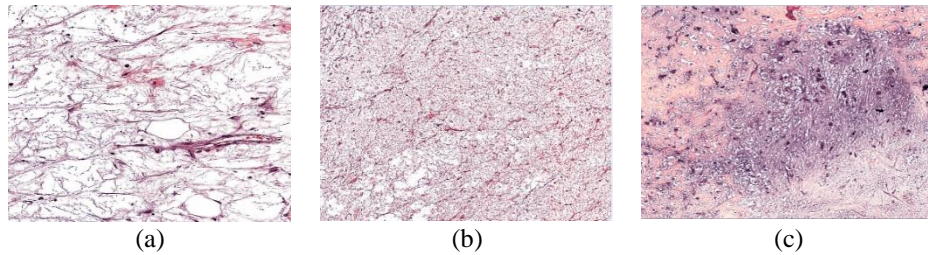


Figure 1. Images samples from the used dataset (a) non-tumor sample image, (b) viable tumor sample image, and (c) osteosarcoma tumor

3.2. Grey level co-occurrence matrices

The GLCM is a common technique for extracting texture-based features from images proposed by Haralick *et al.* [23] in their article "textural features for image classification". The GLCM computes the textural association between pixels by applying a second-order statistical procedure to the images. The GLCM uses the adjacency principle in other words any calculated texture value is based on two adjacency pixels. The GLCM continuously records all pairs of neighboring pixel values that appear in all image directions [24]. The mathematical formula for an image's GLCM characteristics is a matrix with the same number of rows and columns as the image's grey values. The elements of this matrix depend on how frequently the two adjacent pixels appear. Based on their surroundings, both pixel pairings can differ. According to the row and column's grey values, these matrix members have second-order statistical probability values. A big transient matrix results from wide intensity levels. Process load as a result is time-consuming [25]. For a single image, four GLCM matrices are built. There are four forms of adjacency; left to right, upper to bottom, upper left to bottom right, and upper right to bottom left. Fourteen textural characteristics based on statistical theory are calculated from the four GLCM matrices. These characteristics include the angular second moment, contrast, correlation, the sum of squares: variance, the inverse difference moment, the sum average, the sum variance, the sum entropy, the difference variance, the difference entropy, information measures of correlation [f12 and f13], and the maximal correlation coefficient [26].

4. THE PROPOSED SYSTEM

The suggested system is divided into five major stages. The first stage is data preparation. The second stage is color normalization to overcome the non-uniform color for the WSI images. The third stage is feature extraction using GLCM which procedure of 13 different features for each image. The fourth and final stage is the classification stage, we use three different classifiers; XG-Boost, SVM, and K-nearest neighbors. The fifth and final stage is to combine the results from the used classifier and perform ensemble voting. Figure 2 shows the overall proposed model structure. Figure 2(a) data preparation stage assign each image to its corresponding class. Figure 2(b) WSI stained image stage tends to enhance the quality of images. Figure 2(c) feature extraction stage tends to extract images' key characteristics, in this work GLCM is used to extract texture features from the images. Figure 2(d) classification stage images are classified with three different classifier, XG-Boost, SVM, and K-nearest. Figure 2(e) ensemble voting stage apply voting on the used classifier.

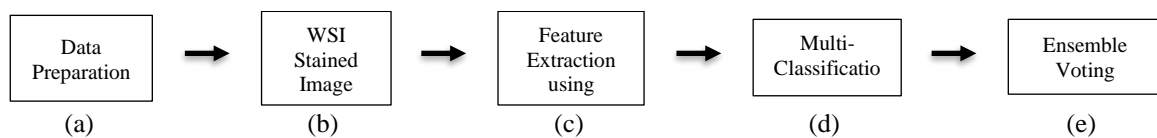


Figure 2. The sequence of the proposed system stages (a) stage 1: data preparation, (b) stage 2: enhance image quality using WSI stained, (c) stage 3: texture feature extraction using GLCM, (d) stage 4: image classification using three different classifier, and (e) stage 5: enhance the accuracy by apply ensemble voting

- Stage 1: the dataset is divided into three classes; non-tumor, viable tumor, and osteosarcoma as shown in Table 1. Use 1,085 images, 810 images used for training and 275 images used for testing.
- Stage 2: normally WSI stained images have non-uniform color dispersion, which affects the feature extraction process so it is important to make color normalization. Image normalization solves the non-

color dispersion problem by reducing color differences and distributing them over all pixels in an image. In this work, the normalization is performed for each image based on hue saturation value (HSV) color space according to Algorithm 1 steps.

Table 1. Data set preparation

Class Number	Class Name	Image samples	
		Train	Test
0	Non-tumor	400	130
1	Viable-tumor	210	82
2	Osteosarcoma- tumor	200	63
Total Samples		810	275

Algorithm 1. Image color normalization

- Step 1: Read image in RGB format.
- Step 2: Convert image to HSV color space.
- Step 3: Threshold the H channel to three distinct regions:
 - Region 0: from 0 to 0.68
 - Region 1: from 0.68 to 0.9
 - Region 2: from 0.9 to 1
- Step 4: Construct image to HSV space
- Step 5: Return image back to RGB format.

- Stage 3: Extract the texture features based on GLCM technique according to Algorithm 2 steps. Figure 3 shows the feature extraction process. The image feature extraction used GLCM to extract the features from WSI gray images. The GLGM extract 14 different feature for each two neighboring pixels in four directions, from left to right, from upper to bottom, from upper left to bottom right, from upper right to bottom left and store the result into matrix feature 1, matrix feature 2, matrix feature 3, and matrix feature 4 respectively. Finally, the average for the obtained features is calculated.

Algorithm 2. Feature extraction

- Step 1: Convert image to gray scale
- Step 2: Extract 14 different statistical feature for each two neighboring pixels from left to right
- Step 3: Store the results into matrix.
- Step 4: Repeat the steps 2 and 3 for each two neighboring in the following directions:
 - Starting from the upper and moving downward,
 - From upper left to lower right,
 - From upper right to bottom left
- Step 5: Calculate the mean of the four matrix.

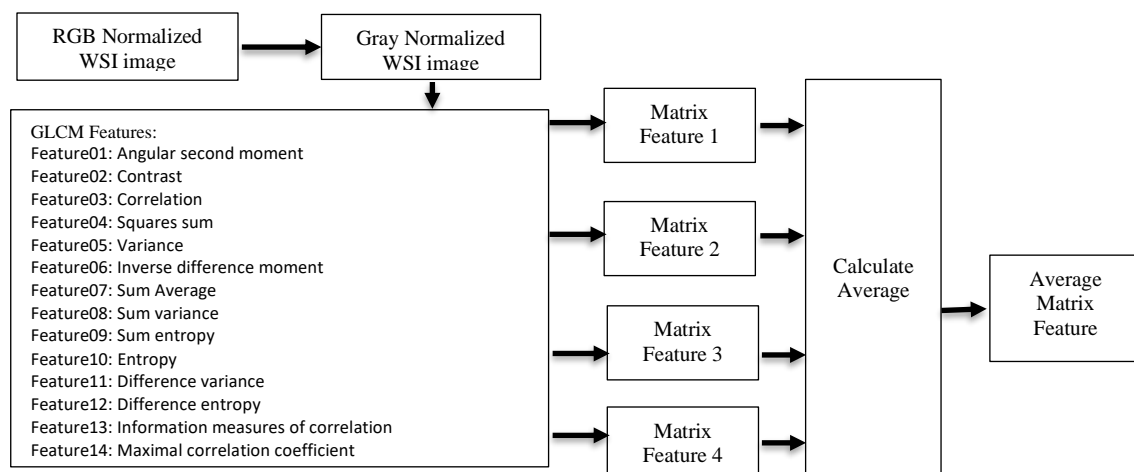


Figure 3. Image feature extraction

- Stage 4 and 5: The features obtained from the previous stage are classified with three different classifiers XG-Boost, SVM, and K-nearest neighbors. The output of these classifiers is combined together to perform ensemble voting. Figure 4 shows the used classification techniques, three different classifiers

XG-Boost, SVM, and K-nearest neighbors are used for classification for average matrix feature that calculated in stage 3 then, the ensemble voting is performed to enhance the classification accuracy.

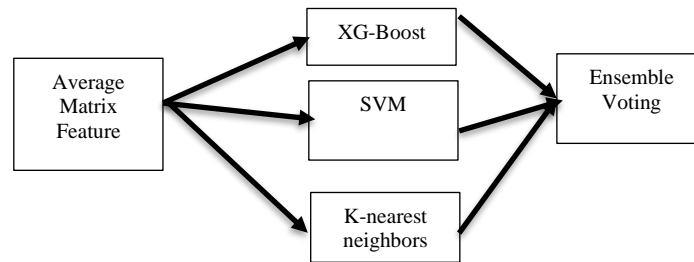


Figure 4. Image classification

5. RESULTS

Table 2 compares between the confusion matrix for the XG-Boost, SVM, K-nearest neighbors and ensemble voting. Class 0 denotes a non-tumor, class 1 a viable tumor, and class 2 an osteosarcoma tumor. Table 3 compares the total accuracy obtained for the XG-Boost, SVM, K-nearest neighbors and ensemble voting algorithms; from the results, it is clear that the best algorithm is ensemble voting with 91.8% accuracy.

Table 2. The confusion matrix and accuracy for XG-Boost, SVM, K-nearest

Input Class \ Predicted Class	0			1			2			3		
	XG-Boost	SVM	K-nearest neighbors	Ensemble voting	XG-Boost	SVM	K-nearest neighbors	Ensemble voting	XG-Boost	SVM	K-nearest neighbors	Ensemble voting
0 (130 image)	136	0	0	135	1	0	134	0	2	136	0	0
1 (82 image)	0	82	0	0	82	0	9	73	0	0	82	0
2 (63 image)	24	0	39	28	1	34	24	0	39	32	0	40

Table 3. Classifier accuracy

Classifier	Accuracy
XG-Boost	91.5%
SVM	89.3%
K-nearest neighbors	87.5%
Ensemble voting	91.8%

6. CONCLUSION

In this study, we present a methodology for identifying different types of osteosarcoma tumors. The proposed model accept WSI image stained with H&E and automatically classify them into three categories; non-tumor, viable-tumor, and osteosarcoma tumor. The GLCM technique is used to extract fourteen image texture features. Three different feature extraction algorithms are used for classification. Finally, the classification is performed by applying ensemble voting. The proposed model achieves 91.8% accuracy.





REFERENCES

- [1] C. de Martel, D. Georges, F. Bray, J. Ferlay, and G. M. Clifford, "Global burden of cancer attributable to infections in 2018: a worldwide incidence analysis," *The Lancet Global Health*, vol. 8, no. 2, pp. e180–e190, Feb. 2020, doi: 10.1016/S2214-109X(19)30488-7.
- [2] D. Crosby *et al.*, "Early detection of cancer," *Science*, vol. 375, no. 6586, pp. 151–152, Mar. 2022, doi: 10.1126/science.aay9040.
- [3] "What is osteosarcoma?," *American Cancer Society*, 2018. Accessed: Aug. 21, 2022. [Online] Available: <https://www.cancer.org/cancer/osteosarcoma/about/what-is-osteosarcoma.html>.
- [4] M. Idoate, J. D. Aquerreta, J. M. Lamo-Espinosa, and M. San-Julian, "A reassessment of the barrier effect of the physis against metaphyseal osteosarcoma: a comprehensive pathological study with its radiological and clinical follow-up correlations," *Diagnostics*, vol. 12, no. 2, p. 450, Feb. 2022, doi: 10.3390/diagnostics12020450.
- [5] T. L. Oncology, "UT Southwestern Medical Center," *UT Southwestern Medical Center*, 2021. Accessed: Aug. 21, 2022. [Online] Available: <https://www.utsouthwestern.edu/>.
- [6] K. Smith, "Osteosarcoma data from UT southwestern/UT dallas for viable and necrotic tumor assessment (osteosarcoma tumor assessment)," *Cancer Imaging Archive*, 2022. Accessed: Aug. 21, 2022. [Online] Available: <https://wiki.cancerimagingarchive.net/pages/viewpage.action?pageId=52756935>.
- [7] S. Wang, D. M. Yang, R. Rong, X. Zhan, and G. Xiao, "Pathology image analysis using segmentation deep learning algorithms," *American Journal of Pathology*, vol. 189, no. 9, pp. 1686–1698, Sep. 2019, doi: 10.1016/j.ajpath.2019.05.007.
- [8] P. Leavey, A. Sengupta, D. Rakheja, O. Daescu, H. B. Arunachalam, and R. Mishra, "Osteosarcoma data from ut southwestern/ut dallas for viable and necrotic tumor assessment [data set]," *The Cancer Imaging Archive*, vol. 14, 2019.





- [9] R. Szeliski, *Computer Vision*. Cham: Springer International Publishing, 2022, doi: 10.1007/978-3-030-34372-9.
- [10] G. Yunchao and Y. Jiayao, "Application of computer vision and deep learning in breast cancer assisted diagnosis," in *ACM International Conference Proceeding Series*, Jan. 2019, pp. 186–191, doi: 10.1145/3310986.3311010.
- [11] G. Boesch, "Top 10 applications of deep learning and computer vision in healthcare," viso.ai. 2023. Accessed: Oct. 06, 2022. [Online] Available: <https://viso.ai/applications/computer-vision-in-healthcare/>.
- [12] P. Dey, "Haematoxylin and eosin stain of the tissue section," in *Basic and Advanced Laboratory Techniques in Histopathology and Cytology*, Singapore: Springer Nature Singapore, 2022, pp. 71–82, doi: 10.1007/978-981-19-6616-3_8.
- [13] Y. Dong, H. Shen, and W. D. Pan, "An interactive tool for ROI extraction and compression on whole slide images," in *3rd IEEE EMBS International Conference on Biomedical and Health Informatics, BHI 2016*, Feb. 2016, pp. 224–227, doi: 10.1109/BHI.2016.7455875.
- [14] G. F. Baker, G. J. Tortora, and N. P. A. Nostakos, "Principles of anatomy and physiology," *The American Journal of Nursing*, vol. 76, no. 3, p. 477, Mar. 1976, doi: 10.2307/3423898.
- [15] J. Wu and M. R. Mahfouz, "Robust x-ray image segmentation by spectral clustering and active shape model," *Journal of Medical Imaging*, vol. 3, no. 3, p. 034005, Sep. 2016, doi: 10.1117/1.jmi.3.3.034005.
- [16] S. Bose, K. Gaynar, and S. P. Singh, "Breast cancer detection by data visualization and feature selection using XG Boost algorithm," in *2022 International Conference on Signal and Information Processing, IConSIP 2022*, Aug. 2022, pp. 1–6, doi: 10.1109/IConSIP49665.2022.10007483.
- [17] S. Mangla, P. Saini, A. K. Jayswal, K. Sanyal, and S. Pal, "An AI based application for cancer diagnosis - an empirical analysis," in *Proceedings of the 13th International Conference on Cloud Computing, Data Science and Engineering, Confluence 2023*, Jan. 2023, pp. 231–236, doi: 10.1109/Confluence56041.2023.10048847.
- [18] X. Dong, Z. Yu, W. Cao, Y. Shi, and Q. Ma, "A survey on ensemble learning," *Frontiers of Computer Science*, vol. 14, no. 2, pp. 241–258, Apr. 2020, doi: 10.1007/s11704-019-8208-z.
- [19] Q. H. Nguyen *et al.*, "Breast cancer prediction using feature selection and ensemble voting," in *Proceedings of 2019 International Conference on System Science and Engineering, ICSSE 2019*, Jul. 2019, pp. 250–254, doi: 10.1109/ICSSE.2019.8823106.
- [20] R. A. Nabid, M. L. Rahman, and M. F. Hossain, "Classification of osteosarcoma tumor from histological image using sequential RCNN," in *Proceedings of 2020 11th International Conference on Electrical and Computer Engineering, ICECE 2020*, Dec. 2020, pp. 363–366, doi: 10.1109/ICECE51571.2020.9393159.
- [21] S. Mahore, K. Bhole, and S. Rathod, "Comparative analysis of machine learning algorithm for classification of different osteosarcoma types," in *2021 12th International Conference on Computing Communication and Networking Technologies, ICCCNT 2021*, Jul. 2021, pp. 1–5, doi: 10.1109/ICCCNT51525.2021.9579556.
- [22] I. Ahmed, H. Sardar, H. Aljuaid, F. A. Khan, M. Nawaz, and A. Awais, "Convolutional neural network for histopathological osteosarcoma image classification," *Computers, Materials and Continua*, vol. 69, no. 3, pp. 3365–3381, 2021, doi: 10.32604/cmc.2021.018486.
- [23] A. Humeau-Heurtier, "Texture feature extraction methods: a survey," *IEEE Access*, vol. 7, pp. 8975–9000, 2019, doi: 10.1109/ACCESS.2018.2890743.
- [24] Gogul Ilango, "Texture recognition using haralick texture and Python," Gogul, 2016. Accessed: Nov. 13, 2022. [Online] Available: <https://gogul.dev/software/texture-recognition>.
- [25] Ş. Öztürk and B. Akdemir, "Application of feature extraction and classification methods for histopathological image using GLCM, LBP, LBGLCM, GLRLM and SFTA," *Procedia Computer Science*, vol. 132, pp. 40–46, 2018, doi: 10.1016/j.procs.2018.05.057.
- [26] "efg's R Notes: EBImage: haralick textural features details," Earlglynn.github.io. 2015. Accessed: Oct. 07, 2022. [Online] Available: <https://earlglynn.github.io/RNotes/package/EBImage/Haralick-Textural-Features.html>.

BIOGRAPHIES OF AUTHORS



Kamel Hussien Rahouma     earned his B.Sc. and M.Sc. in Communications and Electronic Engineering from the Faculty of Engineering, Cairo University in June 1984 and March 1988 respectively. He earned his first doctoral degree in Communications and Electronics Engineering jointly from the University of Kent at Canterbury (England) and Minia University (Egypt) in 1996. In May 2001, he earned his second doctoral degree in Computer Science from the University of Salzburg, Austria. Currently he is a vice dean of the Faculty of Computer Science, Nahda University, Beni Suef, Egypt. He can be contacted at email: kamel_rahouma@yahoo.com.



Ahmed Salama Abdellatif     earned his B.Sc. in Communications and Electronic Engineering from the Faculty of Engineering, Cairo University in June 2003. He earned his Diploma in Computer Science from Institute of Statistical Studies and Research, Cairo University in 2014. He earned his M.Sc. in Electrical Engineering from the Faculty of Engineering, Al-Azhar University in 2016. Now he has worked as a Software Analysis Team Leader at the Egyptian Space Agency. He is experienced in satellite ground stations, data analysis, parallel programming and artificial intelligence systems. He can be contacted at email: ah_salama_eng_eg@yahoo.com.